Materials Today Advances 17 (2023) 100344

Contents lists available at ScienceDirect

Materials Today Advances

journal homepage: www.journals.elsevier.com/materials-today-advances/

Hybrid materials with continuous mechanical property gradients that can be 3D printed

Gloria Young [a], Francesca Tallia [a], Jeffrey N. Clark [b], Manishankar Chellappan [a], Oriol Gavalda-Diaz [a], Enric Juan Alcocer [a], Silvia A. Ferreira [c], Sara M. Rankin [c], Joshua P. Clark [d], John V. Hanna [d], Jonathan R.T. Jeffers [b], Julian R. Jones [a, *]

[a] Department of Materials, Imperial College London, South Kensington Campus, London, SW7 2AZ, UK
[b] Department of Mechanical Engineering, Imperial College London, South Kensington Campus, London, SW7 2AZ, UK
[c] National Heart and Lung Institute, Imperial College London, South Kensington Campus, London, SW7 2AZ, UK
[d] Department of Physics, University of Warwick, Gibbet Hill Road, Coventry, UK

ARTICLE INFO

Article history:
Received 28 September 2022
Received in revised form
14 December 2022
Accepted 3 January 2023
Available online 20 January 2023

Keywords:
Hybrid
Gradient materials
Mechanical properties
Intervertebral disc

ABSTRACT

Here, we show tough materials with continuous composition and stiffness gradients, without interfaces between regions, using inorganic/organic hybrid materials that can also be 3D printed. Sol-gel hybrid materials have interacting and interpenetrating organic and inorganic co-networks and can deliver a synergy of the properties of those constituents. Their mechanical behaviour can be tuned through inorganic/organic content and cross-linking density. We describe hybrids of covalently linked silica-poly (tetrahydrofuran) (SiO_2/PTHF) that show an unprecedented range of mechanical properties. SiO_2/PTHF hybrids were formed with different silica contents, producing materials ranging from elastomeric to glassy, with a compressive stiffness at 10% strain of between 2 and 200 MPa: at an SiO_2 content of 9 wt%, hybrids show a failure stress in compression of 8 MPa, at 70% strain, and tensile strength of 2 MPa at 80% strain. Gradual sol-gel gelation was employed to generate monoliths with composition and stiffness gradients without visible joins or points of weakness, and for development of 'inks' for additive manufacturing of 3D structures through direct ink writing. Monoliths with gradients were at least as strong, in tension and compression, as those made by casting a single sol. Cytocompatible materials with seamless stiffness gradients will have many applications: one is biomimicry of natural cartilaginous structures of the body, such as the intervertebral disc, which has a natural radial stiffness gradient.

1. Introduction

Zonal structures with stiffness gradients are needed to mimic the structure and properties of natural constructs, such as the intervertebral disc (IVD) [1–3]. This requires the synergy of a material with tuneable mechanical properties, to match the stiffness of the different zones of the structure, and the ability to form a continuous, graded structure without weak interfaces between zones. Graded stiffness structures have been achieved with soft materials, such as hydrogels [4] by employing density differences [5], through variation in hydrogel crosslinker [6] and the degree of polymerisation [7]. Low strength hydrogels have been joined with a 50-fold difference in the initial compressive modulus (up to a maximum of the order of 100 kPa) [8], but without systematic measurement of strength and the stress distribution around the interface. Similarly, a stiffness gradient in polyurethane was achieved using a variation in crosslinking density [3], measuring relative variation in mechanical properties through the sample. Hydrogel mechanical properties are often lower that required for structural applications, including cartilage or bone replacement devices, even if double networks are employed [9–12]. The tendency for hydrogels to swell is also not appropriate for many applications. Composite materials are also proposed for the formation of a stiffness gradient [13], for example through the diffusion of nanoparticles [14] through the polymer matrix. However,

Abbreviations: CROP, cationic ring opening polymerisation; DIC, Digital Image Correlation; GPTMS, glycidoxypropyl trimethoxysilane; I/O, Inorganic/organic ratio; IVD, intervertebral disc; PCL, poly(caprolactone); PTHF, polytetrahydrofuran; TEOS, tetraethoxysilane.

* Corresponding author.
E-mail address: julian.r.jones@imperial.ac.uk (J.R. Jones).

https://doi.org/10.1016/j.mtadv.2023.100344

distribution of the particles throughout the matrix is challenging and a lack of bonding between the particles and the matrix often leads the mechanical properties of composites to fall short of theoretical values.

Inorganic-organic hybrid materials have the advantage of finer scale interactions between inorganic and organic components, plus bonding between the networks can be readily achieved [15]. Sol-gel hybrid materials are assembled of intimately mixed co-networks of organic and inorganic components, but above the nanoscale, sol-gel hybrids appear as single phase materials, often transparent, with continuous chemical and physical properties [16], distinguishing them from composites. There is large scope for tailoring their properties through the choice of polymer, inorganic to organic ratio (I/O) and the type of bonding between the co-networks [15]. We hypothesise that hybrid materials can be a successful alternative for the formation of a graded stiffness structure with a large stiffness range and that the gradual gelation of the sol can be utilised to form a continuous structure, by layering sols of different compositions, leaving no interfaces between the regions of different stiffness.

The organic component of the hybrids can be derived from natural polymers [17–21], however, synthetic polymers offer greater reproducibility and control of the organic-inorganic covalent coupling [22]. This is of particular importance in biological applications where a biomaterial should match the mechanical properties of the surrounding tissue, and where each medical device produced must be precisely manufactured to the same specifications. SiO_2-poly(tetrahydrofuran)-poly(caprolactone) (SiO_2/PTHF/PCL-diCOOH) hybrids synthesised by in situ cationic ring opening polymerisation (CROP) of tetrahydrofuran (THF) have covalent bonding between the silica and polymer chains, mediated by glycidoxypropyl trimethoxysilane (GPTMS) crosslinker, and can show compressive behaviour similar to cartilage tissue [23]. The PTHF constituent is of interest as a co-polymer for biomedical applications, in part due to its high flexibility [24,25], as demonstrated in other hybrid systems [26]. Herein, the simultaneous CROP reaction was utilised to form a non-degradable (PCL-free) silica/PTHF (SiO_2/PTHF) with covalent coupling (Class IV hybrid system [15]), which has previously been demonstrated to combine strong and tough mechanical properties [27].

To further create a graded stiffness structure with a hybrid material, tuning of the mechanical properties is required. This tuneability has been achieved through various methods including control of the hybrid coupling agent [28], the polymer backbone [29] and architecture [30], nanoparticle size and I/O ratio [27,31]. Changing the inorganic/organic ratio has resulted in a ten-fold change in both the compressive strength of SiO_2-poly(-caprolactone-*co*-GPTMS) [32] and in the tensile strength of SiO_2/PTHF/PCL-diCOOH hybrids [23]. However, previously reported hybrid materials have not been produced with gradients of properties.

The SiO_2/PTHF hybrid materials presented here are bouncy and compressible and are of particular interest due to the similarity in properties with cartilage tissue. Tuneability of this highly elastomeric material system was investigated and a sol-gel synthesis method was developed to form materials with a gradation in mechanical properties, the sol was tailored for direct 3D printing and cytocompatibility was demonstrated.

2. Materials and methods

2.1. Hybrid synthesis

Materials were obtained from Sigma UK and VWR UK and used as obtained without further purification. SiO_2/PTHF hybrids were prepared by a two-pot synthesis, adapting the method developed by Tallia et al. [23,33], without the addition of poly(ε-caprolactone). Inorganic precursor solution was prepared by hydrolysis of tetraethoxysilane (TEOS) in deionised water with 1 M hydrochloric acid catalyst (3:1 vol% in water) for 1 h. The molar ratio of water was 4:1 TEOS and 3:1 GPTMS. Separately, the CROP of THF monomer in 100:1 GPTMS ratio was initiated using Boron trifluoride diethyl etherate catalyst with molar ratio $BF_3{\cdot}O(C_2H_5)_2$:GPTMS of 1:4. 10 min after catalyst addition, the TEOS solution was added to the polymerisation reaction pot to form the hybrid sol, mixed, sealed and aged for three days at 40 °C, after which excess THF was allowed to evaporate (10–14 days). Hybrids were prepared in a range of compositions denoted by their TEOS/GPTMS molar ratio in the format Si(TEOS/GPTMS)-PTHF (*e.g.* Si2.5-PTHF for a TEOS:GPTMS ratio of 2.5:1), with final silica contents from 3 to 44 wt% SiO_2, of which 7 intermediary compositions (Si1, 1.75, 3.75, 7.5, 10, 20-PTHF in compression and Si1, 1.75, 2.5, 3.75, 5-PTHF in tension) were tested in this work.

To form layered samples, a second hybrid sol which may be of different composition was added at ageing time, $t_{age} = 2$ h, 1 day, 3 days. In the case of cylindrical samples for compression testing, the second solution was poured on top of the first in a half-full mould. For tensile test specimens, half of the hybrid sol from a disc mould of diameter = 15 cm was removed at 2 h ageing, leaving a semi-circle of the first hybrid, after which the second solution was added to the empty half either directly or after resealing for 1 or 3 days.

2.2. 3D extrusion printing

The Si5-PTHF composition was stirred for longer to allow evaporation of excess THF and transferred to 3 mL Luer-lock syringe (VWR) with tapered tip, internal diameter 0.20 mm (Nordson EFD). 3D porous scaffolds were printed by Direct Ink Writing, using a Robocaster with Robocad software (3d Inks LLC), at 8 mm s^{-1}, extrusion ratio of 0.0012, z spacing 0.21–0.24 mm staggered at 8-layer intervals and strut spacing of 0.60 mm, at room temperature. The Robocaster adjusted applied force to achieve constant extrusion rate. After printing, scaffolds were aged and dried at 40 °C as for bulk samples.

2.3. Characterisation of hybrids

Samples were prepared for solution state ^{1}H Nuclear magnetic resonance (NMR) spectroscopy (400 MHz, $CDCl_3$) by dilution of a 100 μL aliquot from the reaction before and after the catalyst in 600 μL $CDCl_3$. Solid state ^{29}Si magic-angle-spinning (MAS) NMR was carried out on machined monolithic samples at 7.05 T (^{29}Si Larmor frequency 69.62 MHz) using a Varian/Chemagnetics InfinityPlus-300 spectrometer. Both single pulse MAS and cross polarisation (CPMAS) experiments were performed at a MAS frequency of 5 kHz using a Bruker 7 mm HX probe. The degree of condensation was calculated from **Equation (1)** [21].

$$D_c = \left(\left[\frac{4Q^4 + 3Q^3 + 2Q^2}{4} \right] + \left[\frac{3T^3 + 2T^2 + T^1}{3} \right] \right) \quad \text{x } 100\% \tag{1}$$

Final inorganic content was determined by Thermogravimetric analysis (TGA) (Netzsch Jupiter STA 449C) at a heating rate of 10 °C min^{-1} from 20 to 800 °C. Thermo Scientific Nicolet iS10 Fourier-transform infrared (FTIR) spectrometer equipped with Smart Golden Gate for Single-Reflection Diamond Attenuated Total Reflectance Analysis with OMNIC software was used to give spectra

in the range 4000–400 cm^{-1}. FTIR wavenumber (ν): $\nu_{asymmetric}$ (Si–O–Si), ν(Si–O–C), ν(C–O–C) overlapping ~ 1100-1000 cm^{-1}; $\nu_{symmetric}$ (Si–O–Si) ~ 800 cm^{-1}; ν(Si–OH) ~ 950 cm^{-1}; ν(CH_2) ~ 3000-2800 cm^{-1}. Normalised to the highest band at 1100-1000 cm^{-1} (Si–O–Si symmetric and overlapping Si–O–C, C–O–C).

2.4. Mechanical testing

Uniaxial tensile testing to failure was carried out according to ASTM D1708–13 on samples of length x width x thickness ≃ 45 × 10 x 0.5–2 mm (measured for each sample) with 25 mm exposed length, using Bose Electroforce Series III machine fitted with 440 N load cell, in displacement control at a rate of 1 mm min^{-1}. Minimum 5 valid repeats (samples failing at grips were excluded). For samples made by layering sols, the join was located at the centre of the sample perpendicular to the applied force. Stress relaxation was carried out on samples of the same dimension to 30% of the strain to failure at 10 mm min^{-1} and held for 1 h. Uniaxial compression testing and cyclic compression testing (10 cycles) were carried out on cylindrical samples of height x diameter ≃ 15 × 10 mm using Zwick machine fitted with 1 kN load cell, in displacement control at a rate of 1 mm min^{-1}.

2.5. Digital Image Correlation (DIC)

DIC was conducted by creation of an ink pattern by hand on the surface of the hybrid, photographed every 2 s during compression tests. ImageJ was used to process images and GOM Correlate 2018 to produce strain maps with surface component facet size = 100 pixels, point distance = 40 pixels (parameters optimised using stationary images).

2.6. Cell studies

As one of the intended applications of the material is a cartilage replacement, cytotoxicity of Si5-PTHF and cell attachment to its surface was tested using chondrogenic ATDC5 (cell line from American Type Culture Collection). Cytotoxicity was evaluated according to ISO 10993–5, using an MTT assay of the cells exposed to the dissolution products of the material. Samples were prepared and references selected according to ISO 10993–12; negative control was a high-density polyethylene film and positive control polyurethane film containing 0.1% zinc diethyldithiocarbamate (Hatano Research Institute). Cell metabolic activity was evaluated using RealTime-Glo MT Cell Viability Assay (Promega) over time. Then, for cell attachment, ATDC5 cells were seeded on sterilised 25 mm^2 hybrid squares at low (1×10^4 cells cm^{-2}) and high density (5×10^4 cells cm^{-2}) and incubated under standard culture conditions with Dulbecco's Modified Eagle's Medium/Nutrient Mixture F-12 Ham supplemented with 1 vol% antibiotic-antimycotic solution and 1 vol% L-Glutamine (all from Sigma) and 10 vol% Fetal Bovine Serum (Gibco). At day 10, the cell cytoskeleton (actin and tubulin) was stained, as previously described [34,35], and imaged in a Leica SP8 inverted confocal laser scanning microscope. Statistical analyses were carried out using a non-parametric Kruskal-Wallis test followed by Dunn's multiple comparison test for multiple comparisons with GraphPad Prism version 7.

3. Results and discussion

Class IV hybrids composed of co-networks of PTHF and silica were produced (Fig. 1a) with highly elastomeric properties (they bounce – see supplementary video). The schematic in Fig. 1a depicts that the PTHF chains formed in situ and covalently bonded to nanometre scale regions of silica (via GPTMS crosslinker). The silica formed through the hydrolysis of TEOS and subsequent polycondensation, forming a silicate network. Above the nanoscale, a homogeneous material was formed, as evidenced by bright field Transmission Electron Microscopy (TEM), Fig. 1a inset. Previous TEM imaging of PCL-SiO_2 hybrids, made using the same acidic TEOS hydrolysis to form the silica sol, showed similar homogeneity, with approximate size of silica regions of 5 nm [36,37]. In the polymerisation mechanism, the GPTMS acts as the initiator: when its epoxide ring is activated by the $BF_3 \cdot O(C_2H_5)_2$ catalyst, the resulting intermediary is subject to nucleophilic attack by THF monomers. The product is also susceptible to nucleophilic attack by THF monomers, thus a cationic ring opening polymerisation is initiated [33]. Colloidal silica sol, produced by acid-catalysed hydrolysis of TEOS, was introduced into the ongoing polymerisation, where it co-condensed with the alkoxysilane groups of GPTMS. Because GPTMS acts as the initiator of the polymerisation, increasing the amount of GPTMS increased the polymer content of the final hybrid. Therefore, the TEOS:GPTMS ratio was used to control the resulting I/O ratio of the hybrid material.

This mechanism of the formation of the hybrid material was confirmed by a combination of ^{1}H NMR (liquid state), solid state ^{29}Si NMR and FTIR. ^{1}H NMR of the polymer solution prior to addition of silica sol, before and after $BF_3 \cdot O(CH_3)_2$ catalyst addition (Fig. 1b, top and bottom respectively), confirmed the opening of the epoxide ring of the GPTMS because peaks at $\delta = 3.13, 2.77, 2.60$ ppm (shaded region), attributed to hydrogens on the epoxide carbons, were seen before addition of catalyst but were not present after. The formation of PTHF is indicated by the additional peaks appearing at lower chemical shift to those of THF at δ 1.85 and 3.76 ppm [38] after catalyst addition. Solid state ^{29}Si MAS NMR (Fig. 1c) detected $Si(O–Si)_n(OH)_{4-n}$ (Q^n) and $C–Si(O–Si)_n(OH)_{3-n}$ (T^n) speciation with chemical shifts centred at $\delta \sim -110$ and −60 ppm, respectively. In these cases, Q^n represents silica tetrahedron with n bridging oxygen (Si–O–Si) bonds ($n \leq 4$) and T^n represents -O^n-Si-C- ($n \leq 3$) moieties [39]. The ^{29}Si resonances assigned to T^3 species at $\delta \sim -64$ ppm arise from condensed silica attached to GPTMS, while those assigned to Q^4 species at $\delta \sim -110$ ppm represent from fully condensed silica emanating from the TEOS source. The simultaneous observation of both T^3 and Q^4 species indicates the co-condensation of silica groups from GPTMS with those of hydrolysed TEOS, thus indicating the formation of a covalently bonded inorganic-organic network. The degree of condensation, D_c (**Equation (1)**), [21] was 90.6%, which is consistent with other hybrid materials prepared via the sol-gel method using GPTMS as a coupling agent [19,40].

FTIR confirmed the compositional changes controlled by the TEOS:GPTMS ratio of the synthesis (Fig. 1d): a relative increase in the absorption of the Si–O–Si symmetric stretch at 800 cm^{-1} and the Si–OH stretch at 950 cm^{-1} was observed as the TEOS:GPTMS ratio increased, with a corresponding decrease in the relative absorption of the organic bands at 2800-3000 cm^{-1} [41,42].

By varying the ratio of silica source (TEOS) to crosslinker (GPTMS), hybrids with a final inorganic content of between 3.6 and 44.4 wt percentage (wt%) SiO_2 were produced using TEOS:GPTMS ratios ranging from 0 (no TEOS added, so all SiO_2 was derived from GPTMS) to 20, which are denoted as Si0-PTHF and Si20-PTHF respectively. Monolithic hybrid samples with higher silica content than 45 wt% (Si20-PTHF) tended to crack during drying. PTHF and the organic portion of GPTMS form the total organic content, and the remaining inorganic content was silica, derived from the TEOS and the inorganic portion of GPTMS. Since the THF was in excess and some evaporated during drying, the final inorganic content was determined by TGA. In hybrid samples formed from a single sol, the inorganic content varied by around 1 wt% across a bulk sample (height 15 mm, diameter 10 mm, Fig. 1e). The gradual gelation of

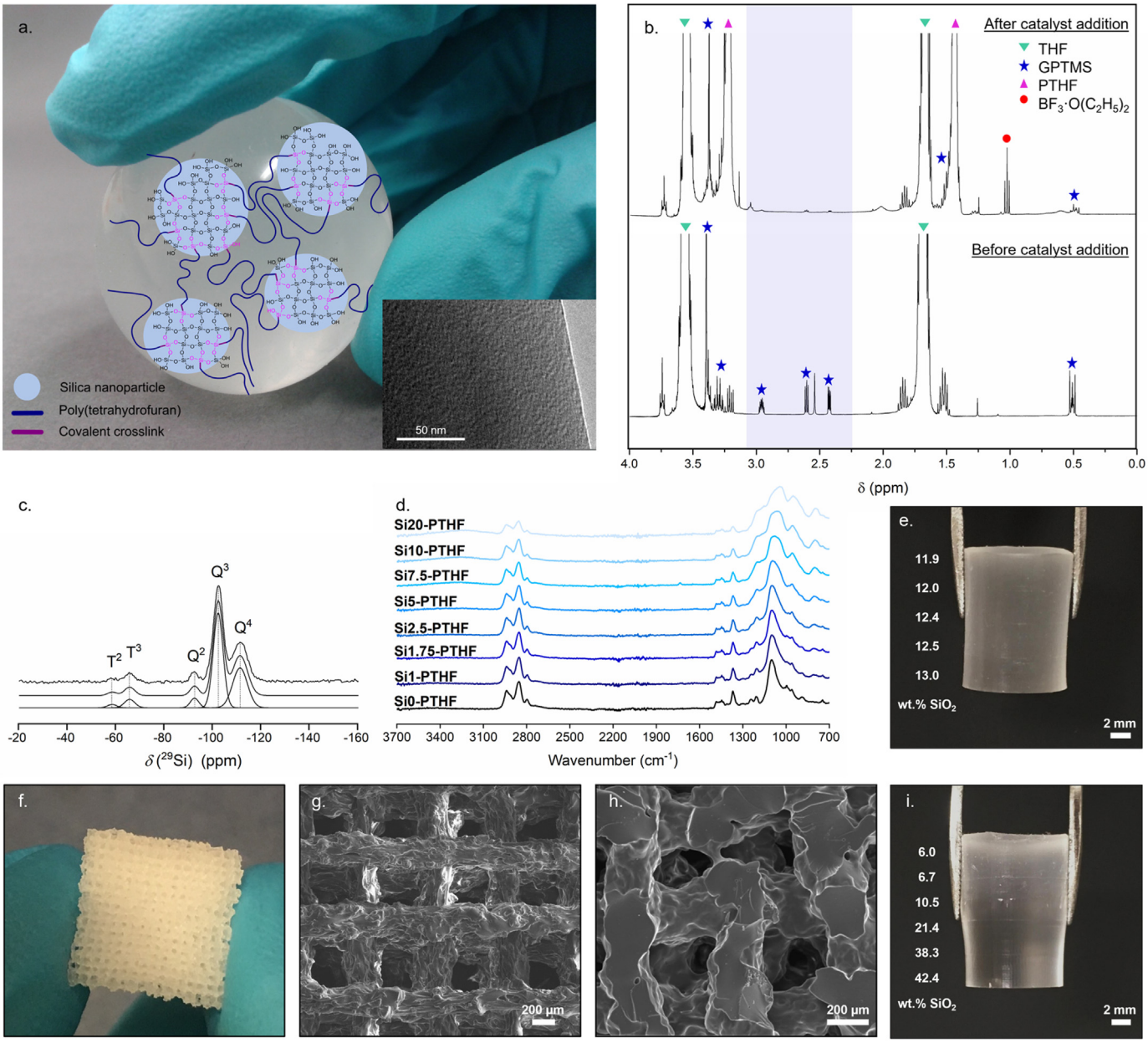

Fig. 1. (**a.**) Photograph of a silica/PTHF hybrid with a schematic of its co-network structure of 1–2 nm diameter silica domains covalently bonded to PTHF chains via a GPTMS crosslinker, with a TEM image (inset) confirming homogeneity above the nanoscale. (**b.**) ^{1}H NMR provided evidence of in situ CROP of PTHF through opening of the GPTMS epoxide ring after the addition of $BF_3{\cdot}O(C_2H_3)_2$ catalyst; (**c.**) FTIR showed changes in relative proportions of the Si–O–Si symmetric vibration (800 cm^{-1}) and CH_2 bands (2800-3000 cm^{-1}) with respect to the TEOS:GPTMS ratio denoted in sample codes, i.e. Si20-PTHF had TEOS:GPTMS ratio of 20 (inorganic content of 44.4 wt% SiO_2); (**d.**) solid-state ^{29}Si NMR quantified relative proportions of T^n (-O_n-Si-C-) and Q^n (-Si-O_n-) species at different condensations in a hybrid with 31 wt% SiO_2 (Si15-PTHF). (**e.**) A photograph of a cast cylindrical monolith of the Si2.5-PTHF composition showing the inorganic content (after drying) measured by TGA in 2 mm sections. (**f.**) Gradual gelation of the hybrid sol was used for additive manufacturing of 3D porous scaffolds using an "ink" of the Si5-PTHF composition, through direct ink writing; (**g.**) SEM images of the scaffolds showed aligned pores of ~300 μm diameter from a top view and (**h.**) the layer-by-layer fusion of printed layers through the horizontal cross-section. (**i.**) Monolithic hybrids with a gradient of silica content and corresponding mechanical property gradient were produced by sequentially layering sols of different compositions (from top: Si1-PTHF, Si2.5-PTHF, Si20-PTHF), after 2 h ageing.

the hybrid sol was exploited as a printing window for direct ink writing of porous scaffolds from the hybrid sol of Si5-PTHF composition (Fig. 1f). To explore their potential use as tissue scaffolds, scaffolds were directly printed in aligned lattices, by extrusion of the viscous sol, giving line-of-sight channels with diameter of around 200 μm (scaffold top view, Fig. 1g). Successive layers (struts) fused together, forming a continuous structure at the intersections through gelation, (horizontal section, Fig. 1h). Optimising printing parameters for Si5-PTHF ink formulation produced scaffolds with a channel size of 300 μm and inorganic content of 27.7 wt%.

The gradual gelation of the hybrid sols (of the same or different composition) also allowed monolithic cylinders to be produced with composition stiffness gradients by layering. Successive sols must be layered within the 3-day ageing process, creating a single crack-free sample with a variation in silica content along its length and without a visible interface between them. Fig. 1i shows a hybrid sample (height ~10 mm) formed with a difference of 38 wt% SiO_2 between either end.

Increasing inorganic content of SiO_2/PTHF hybrids changes their

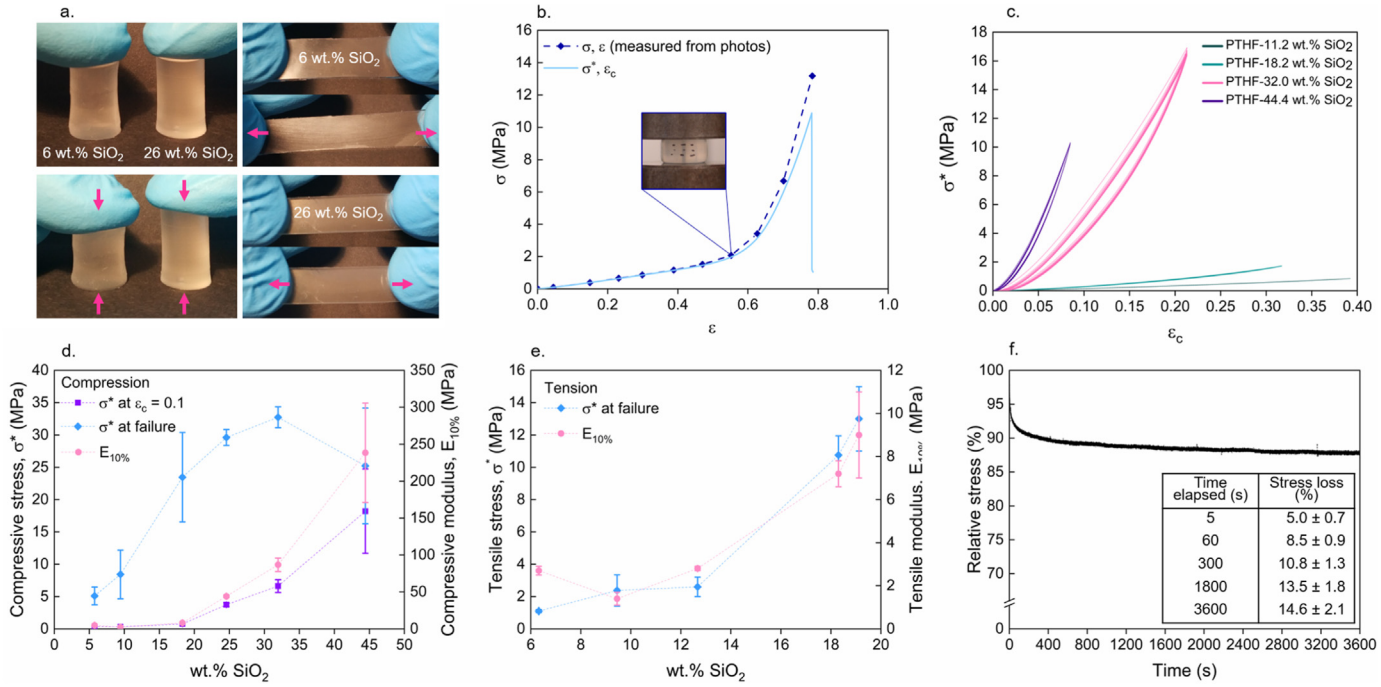

Fig. 2. (**a.**) The mechanical properties of silica/PTHF hybrid monoliths (formed from a single sol, of one composition) can be tuned by control of the inorganic-organic ratio, illustrated by the difference in deformability by hand for 6 and 26 wt% SiO_2. (**b.**) A plot of true stress, σ*, against engineering strain, ε_c, gives close agreement with the stress and strain values calculated from instantaneous sample dimensions throughout the test for Si5-PTHF sample, measured from images. (**c.**) Cyclic testing to 30% of failure strain shows recoverable strains over the composition range. (**d.**) Compressive stiffness (measured at 10% engineering strain) increased as silica content increased, as did the strength, up to a limit of ~30 wt% SiO_2. (**e.**) In tension, the same trend was seen, only measured up to 20 wt% SiO_2 due to testing limitations. (**f.**) Stress relaxation over 1 h was approximately 15%.

properties from those of an elastomeric material, which can be compressed easily with two fingers and undergoes large deformations, to those of a glassy material that fails by brittle fracture, illustrated by the deformation of hybrids made with 6 and 26 wt% SiO_2 samples by hand in Fig. 2a.

This shows the mechanical properties of hybrid materials can be tailored [15] and is consistent with the increasing contribution to the properties from silica as the wt% SiO_2 increased. Hybrid samples of a single composition (25 wt% SiO_2) showed J-shaped stress-strain curves under compression, producing large extensions for small initial stresses, owing to progressive alignment of polymer chains. True stress and engineering strain values were used for calculation of mechanical properties as they matched closely to the stress and strain calculated from instantaneous sample dimensions measured by image analysis (Fig. 2b). At silica contents below around 30 wt%, samples can undergo large recoverable strains in compression, as shown in Fig. 2c, to 10 cycles at 30% engineering strain. This is an important property when considered for tissue replacement applications and interesting because the shape of the stress-strain curves also matches that of cartilage [43], which shows elastomeric behaviour and is hard to replicate in synthetic materials whilst maintaining sufficient mechanical strength. The hybrids show good mechanical stability including at high polymer content, with a stress relaxation of less than 10% over 1 min and 15% over 1 h, after extension to 30% of the failure strain (Fig. 2c).

Compressive strength at failure increased from 5 ± 1 MPa to 33 ± 2 MPa as silica content increased up to a limit of around 30 wt% SiO_2 (Fig. 2d). No further increase in strength occurred above 30 wt % SiO_2, which may be due to the interconnection of the silica network at high I/O ratio leading to an increase in brittleness. The strength was greater than that for similar SiO_2/PTHF Class II hybrids, of the same composition but without covalent bonding between the inorganic and organic components [31], and other authors found a similar sweet spot in the balance between strength and flexibility at around 12 wt% SiO_2 [27]. Although compressive strain at failure decreased with increasing silica content, all samples showed elastomeric behaviour: even samples of 44 wt% SiO_2 reached 13% strain before failure.

Due to the high failure strains, the compressive stress and stiffness at 10% strain were calculated for practical comparison. The compressive stiffness at 10% strain ($E_{10\%}$), increased from 2 to 240 MPa over the composition range from 6 to 44 wt% SiO_2. Hence, the mechanical properties can be tailored over a 100-fold difference in stiffness via control of the inorganic content of the hybrid. SiO_2/PTHF/PCL-diCOOH hybrids, synthesised as described by Tallia et al. [23], also show the same order of magnitude variation in stiffness (Table 1). Previous SiO_2/poly(tetrahydropyran)/PCL hybrids showed a three-fold increase in Young's modulus and six-fold increase in storage modulus when increasing from 15.1 to 36.5 wt% SiO_2 [29]. In tension, the stiffness and failure stress increased as silica content increased from 2.7 ± 0.2 MPa and 1.1 ± 0.1 MPa respectively at 6 wt % SiO_2 to 9 ± 2 MPa and 13 ± 2 MPa at 19 wt% SiO_2 (Fig. 2e), giving a smaller tuneable range, over a smaller range of I/O compositions tested. This is consistent with previous work that found an ultimate tensile strength of 1.3 MPa at 12.8 wt% SiO_2 [27].

PTHF has previously been shown to be non-cytotoxic and showed little evidence of degradation over 3 months [44,45] and owing to the highly elastomeric behaviour of this SiO_2/PTHF hybrid system, here one composition (Si5-PTHF) was additionally tested for cytocompatibility and cell attachment of ATDC5 to the surface. All tested concentrations of the hybrid material extract solution showed chondrogenic cells metabolic activity ≥90%, thereby complying with ISO 10993−5 for non-cytotoxicity. There was no significant difference among all tested concentrations, blank and negative (non-cytotoxic) control but all were shown to be significantly different ($p < 0.01$) to the positive (cytotoxic) control

Table 1
Mechanical properties (tension and compression) of SiO_2/PTHF hybrids denoted by Si(TEOS/GPTMS ratio)-PTHF with different inorganic contents (wt.% SiO_2), and *SiO_2/PTHF/PCL-diCOOH* hybrids for comparison. σ* is true stress, ε is nominal strain, ε* is true strain, $E_{10\%}$ is the stiffness at 10% strain.

Composition	wt.% SiO_2 ±2	*Compression*			*Tension*		
		σ* at failure (MPa)	ε at failure (%)	$E_{10\%}$ (MPa)	σ* at failure (MPa)	ε* at failure (%)	$E_{10\%}$ (MPa)
Si1-PTHF	6	5.1 ± 1.4	67 ± 3	4.7 ± 0.6	1.1 ± 0.1	34 ± 5	2.7 ± 0.2
Si1.75-PTHF	10	8.4 ± 3.7	72 ± 4	2.2 ± 0.3	2.4 ± 1.0	80 ± 15	1.4 ± 0.3
Si3.75-PTHF	18	24.5 ± 6.9	73 ± 10	8.0 ± 0.4	10.8 ± 1.2	60 ± 3	7.2 ± 0.6
Si5-PTHF	25	29.6 ± 1.2	73 ± 5	44.1 ± 1.9	–	–	–
SiO_2/PTHF/PCL-diCOOH	*25*	*4.3 ± 1.0*	*20 ± 3*	–	*0.6 ± 0.2*	*4.7 ± 1.0*	–
Si10-PTHF	32	32.7 ± 1.6	35 ± 1	86.7 ± 9.2			
SiO_2/PTHF/PCL-diCOOH	*32*	*12.0 ± 3.0*	*10 ± 2*	–			
Si20-PTHF	45	25.2 ± 8.9	13 ± 4	237 ± 67			
SiO_2/PTHF/PCL-diCOOH	*49*	*7.6 ± 1.2*	*8 ± 1*	–			

(Fig. 3a.). Chondrogenic cells were seeded on the hybrid material, attached to the surface within 2.5 h and remained metabolically active and viable in culture over 14 days, although not proliferating (Fig. 3b.). The staining of the cytoskeleton (actin and tubulin) of the chondrogenic cells at day 10 shows that the cells attached and spread on the surface of the hybrid material (Fig. 3c.). This indicates the potential for SiO_2/PTHF hybrids to be used as implant materials, subject to further investigations.

After understanding the tuneability of the hybrid system over a range of compositions, the next step was to develop a synthesis method for the formation of graded hybrid samples.

Polymerisation of THF continues during the ageing time (3 days sealed), after which THF evaporation can occur and the sample shrinks. A second hybrid solution (of the same or different composition) can be added to the first during this ageing time (t_{age}). To maintain the separation of the component hybrids the minimum t_{age} was set at 2 h so that the solutions have sufficient viscosity to not mix completely. Fig. 4a and b compare the monoliths formed by the layering of two hybrid sols after 2 h ageing; of the same (Si2.5-PTHF/Si2.5-PTHF, Fig. 4a) and different (Si2.5-PTHF/Si7.5-PTHF) compositions (Fig. 4b). No interface was visible after gelation. The variation in silica content through the monolith was measured using TGA after sectioning the monoliths into 2 mm segments. Greater differences in silica content across a 15 mm sample (from 6 to 42 wt% SiO_2) were achieved by layering three hybrid sols of different silica content (Si1-PTHF/Si2.5-PTHF/Si20-PTHF) (Fig. 4c). When this sample was compressed, there was high deformation in the lower silica content region (Fig. 4d), confirming the variation in stiffness through the sample. To isolate the effect of the processing on the interface properties (rather than the difference in composition), two hybrid sols with the same composition were joined at different ageing times, t_{age} = 2 h, 1 day, 3 days, in the form of tensile testing samples. The interface was tested in tension, perpendicular to the applied force (Fig. 4e).

Tensile samples were prepared in an open mould so small differences in solution depth make the join visible, compared to

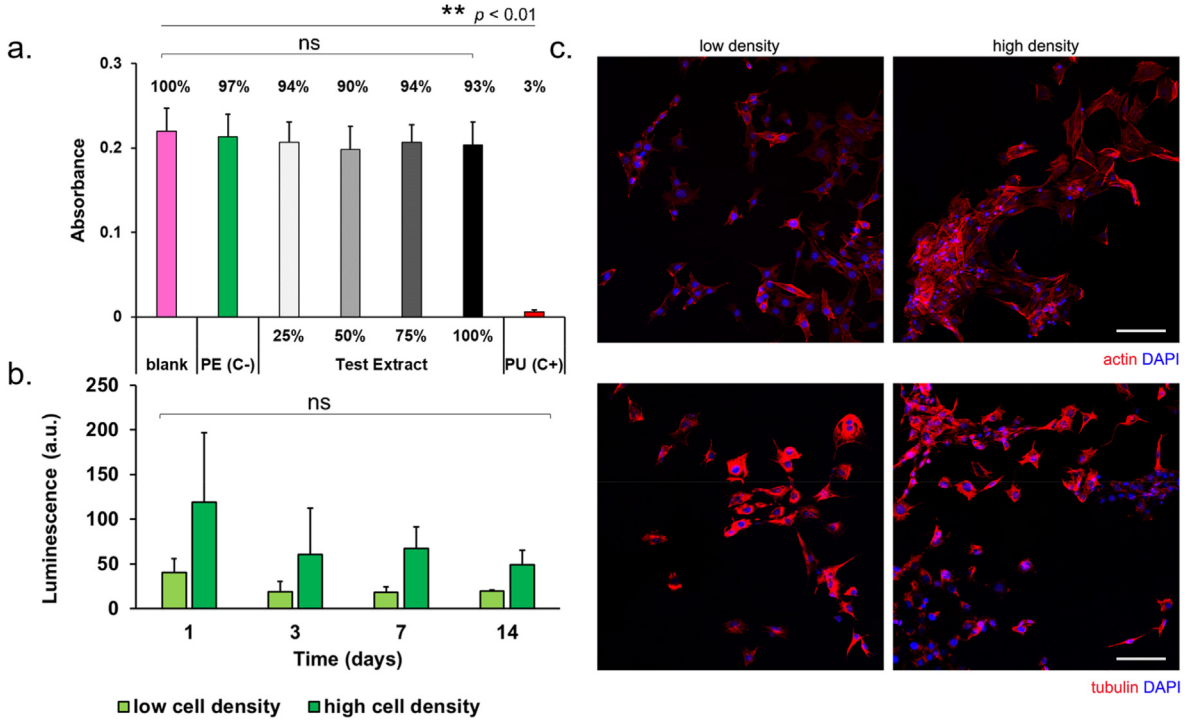

Fig. 3. (**a.**) Si5-PTHF extract solutions are non-cytotoxic to ATDC5 chondrogenic cells (MTT results after 24 h, n = 6). (**b.**) Chondrogenic cells seeded on the hybrid material were metabolically active over time (n = 5). (**c.**) Cytoskeleton (actin and tubulin, red) and nuclei (DAPI, blue) staining of chondrogenic cells seeded on the surface of hybrid material at day 10. Scale bar = 100 μm. (For interpretation of the references to colour in this figure legend, the reader is referred to the Web version of this article.)

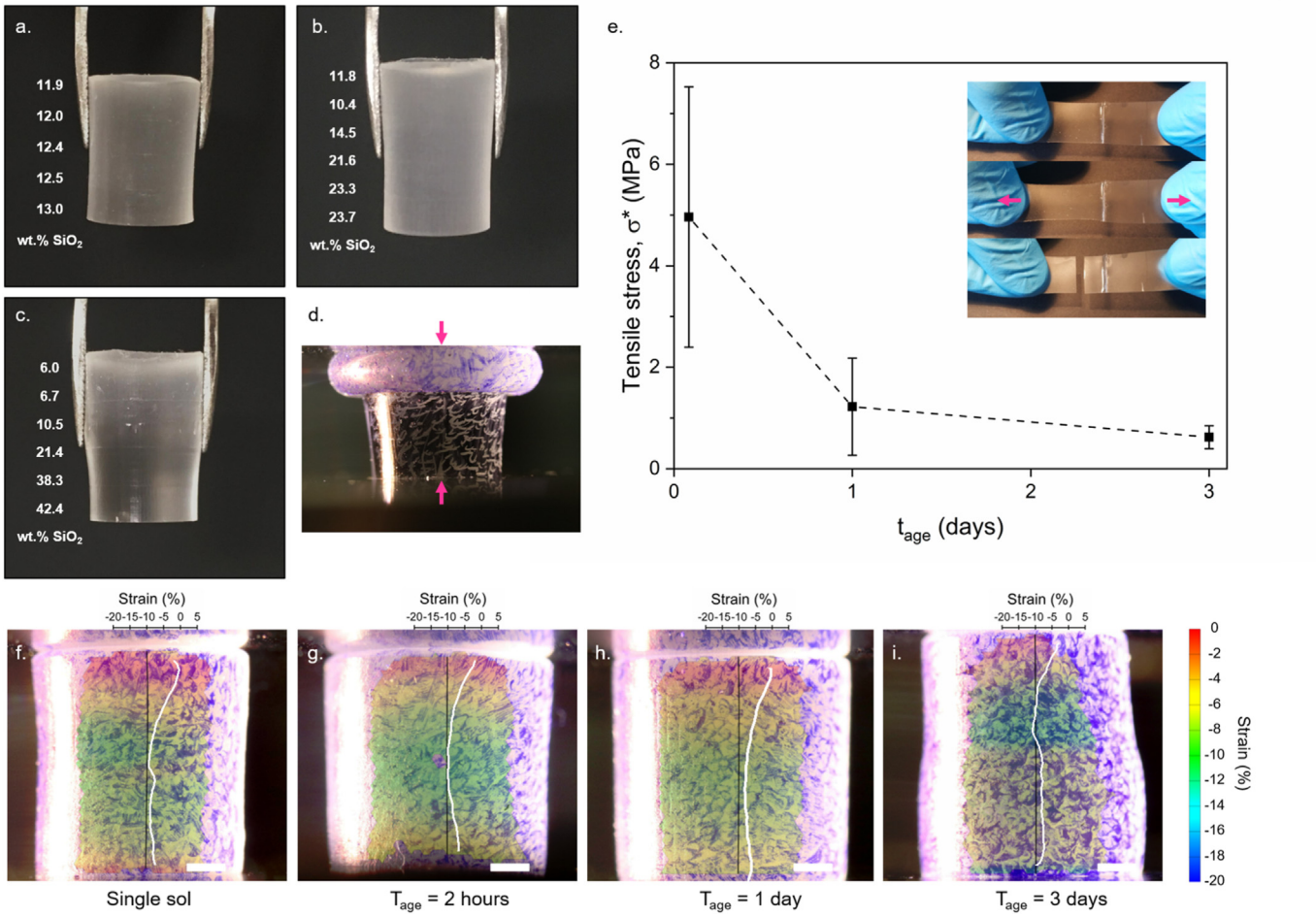

Fig. 4. Mechanical properties of hybrids with continuous gradients. (**a.**) Two hybrid sols of the same TEOS:GPTMS starting ratio (2.5:1) were joined, after 2 h ageing, to form monoliths of constant silica content ~12.5 wt% (<1 wt% difference throughout) and (**b.**) two hybrid sols of different starting TEOS:GPTMS ratio (2.5:1 top, 7.5:1 bottom) formed monoliths with a difference of 12 wt% silica between top and bottom of cylinder. (**c.**) Up to 36 wt% difference in silica was possible by combining three hybrid sols (Si1-PTHF, Si2.5-PTHF, Si20-PTHF) at intervals of 2 h ageing and (**d.**) compression of this monolith made the less stiff upper region deform significantly. (**e.**) A graph of tensile testing of monoliths formed from two hybrid sols of the same composition confirmed that those joined after 2 h of ageing were at least as strong as those formed from a single sol: inset shows Si2.5-PTHF/Si7.5-PTHF joined at 3 days ageing, failure occurs away from the interface in the less stiff region. When DIC showed homogeneous strain distribution in: (**f.**) Si2.5-PTHF samples made from a single sol, (**g.**) for monoliths made of two Si2.5-PTHF sols joined after 2 h ageing and (**h.**) two Si2.5-PTHF sols joined after 1 day. (**i.**) A peak strain as seen close to the interface in monoliths joined after 3 days of ageing. Scale bar = 2 mm. The white line graphs (**f.-i.**) show a plot of the strain value along the central axis of each cylinder (black line).

cylindrical samples. Samples formed from hybrid sols joined at t_{age} = 2 h never failed at the interface (n = 5), including those of different compositions, and were at least as strong as those formed from a single hybrid sol of the same composition. This confirms that layering the sol at 2 h ageing time did not reduce the tensile strength of the material.

For samples formed at t_{age} = 1 day, one out of five samples failed at the interface. Samples joined at t_{age} = 3 days failed at lower average stress: for these samples, failure happened in some cases at the interface because of a concentration of defects due to localised shrinkage. Samples made of different compositions (Si2.5-PTHF/Si7.5-PTHF) show the deformation concentrated in the less stiff region and, when using t_{age} = 2 h, also did not fail at the interface.

The inset of Fig. 4e instead shows a Si2.5-PTHF/Si7.5-PTHF sample formed at t_{age} = 3 days, with a concentration of deformation in the less stiff region (Si2/5-PTHF) and eventual failure away from the join.

Similar strong interfaces have been achieved in zonal hydrogels, including a stiffer zone with modulus of the order of 100 kPa and compressive strength of 2.5 MPa [8]. However, hydrogels are currently limited to low stiffness applications. So, for example, if considering the gels for IVD replacement application the stiffnesses achieved were lower than required (stress in the IVD during weight bearing activity, is approximately 2.3 MPa when lifting 20 kg with rounded back) [46]. Furthermore, there is a lack of systematic measurement of the strength of the interface of the gels.

A significant challenge when forming a graded stiffness structure is achieving an understanding of stress distribution around the joins and its impact on the specimen properties. For this, DIC was used to image the surface strain during compression of cylinders formed from two hybrid sols of the same composition (Si2.5-PTHF/Si2.5-PTHF) joined at t_{age} = 2 h, 1 day and 3 days (Fig. 4g, h, i respectively, shown at 10% engineering strain). DIC uses the correlation between a pattern in a small area (facet) between consecutive images taken at 2 s intervals during the compression test to determine the displacement of that facet and therefore the strain vector. The vertical strain is depicted as a colour scale from red (0%) to blue (−20%) and additionally plotted along the central line of the cylinders (white line trace), to avoid error due to out-of-plane motion of the curved surface. For samples joined at t_{age} = 3

days, a strain concentration is evident at the interface (narrower region of higher strain), whereas when sols are joined at an earlier gelation stage of $t_{age} = 2$ h or 1 day, the longer-range mixing of the sols produced a homogenous strain across the central portion of the cylinder. The strain along the central axis was similar to that seen during compression of cylinders formed from a single hybrid sol of the same composition (Fig. 4f). Hence, combining the evidence of DIC and tensile testing we show that the interface properties can be tailored, and that the formation of an interface does not act as a specimen defect when formed at 2 h ageing. This is an important property of sol-gel hybrid materials.

4. Conclusions

A SiO_2/PTHF hybrid system was presented with highly elastomeric properties, which can withstand large, recoverable compressive strains. The tuneability of the hybrid system was demonstrated in tension and compression, via control of the inorganic/organic ratio. Uniquely, hybrid sols of different composition were layered during the ageing process, producing samples with a gradation of stiffness without visible internal interfaces. Samples formed from two sols of identical composition were of equivalent strength to monolithic samples formed from a single sol, with no strain concentration at the interface. Thus, this constitutes a method for the fabrication of tuneable mechanical property gradients, via variation in the I/O ratio, in which the interfacial properties can also be controlled and optimised. The gradual gelation of the hybrid sol was used for 3D extrusion printing of scaffolds and can find application in biomedical materials and soft robotics.

Author contribution

GY: Conceptualisation, Investigation, Data curation, Writing – original draft preparation; FT: Conceptualisation, Methodology, Writing - reviewing and editing; JNC: Methodology, Investigation, Data curation; MC: Investigation; OG-D: Methodology; EJ-A: Investigation; SAF: Investigation, Data curation, Writing - reviewing and editing; SMR: Funding acquisition, Supervision, Writing - reviewing and editing; JPC: Investigation, Data curation; JVH: Supervision, Writing - reviewing and editing; JRTJ: Funding acquisition, Supervision; JRJ: Conceptualisation, Funding acquisition, Supervision, Writing - reviewing and editing.

Declaration of competing interest

The authors declare that they have no known competing financial interests or personal relationships that could have appeared to influence the work reported in this paper.

Data availability

Data will be made available on request.

Acknowledgements

The authors acknowledge support from the EPSRC (EP/I020861/1 and EP/N025059/1). JVH thanks the EPSRC (grants EP/M028186/1 and EP/K024418/1) and the University of Warwick for partial funding of the solid-state NMR infrastructure at Warwick, and acknowledges additional support for this infrastructure obtained through Birmingham Science City: Innovative Uses for Advanced Materials in the Modern World (West Midlands Centre for Advanced Materials Projects 1 and 2), with support from Advantage West Midlands (AWM) and partial funding by the European Regional Development Fund (ERDF). JRTJ thanks the National Institute for Health and Care Research (NIHR300013). The data that support the findings of this study are available from the corresponding author upon reasonable request from rdm-enquiries@imperial.ac.uk. For the purpose of open access, the author has applied a Creative Commons Attribution (CC BY) licence (where permitted by UKRI, 'Open Government Licence').

Appendix A. Supplementary data

Supplementary data to this article can be found online at https://doi.org/10.1016/j.mtadv.2023.100344.

References

[1] C.K. Lee, N.A. Langrana, J.R. Parsons, M.C. Zimmerman, Development of a prosthetic intervertebral disc, Spine (Phila. Pa. 16 (1991) (1976) S253–S255.
[2] L.J. Nesti, W.J. Li, R.M. Shanti, Y.J. Jiang, W. Jackson, B.A. Freedman, T.R. Kuklo, J.R. Giuliani, R.S. Tuan, Intervertebral disc tissue engineering using a novel hyaluronic acid-nanofibrous scaffold (HANFS) amalgam, Tissue Eng. 14 (2008) 1527–1537, https://doi.org/10.1089/ten.tea.2008.0215.
[3] J.H. Gwynne, M.L. Oyen, R.E. Cameron, Preparation of polymeric samples containing a graduated modulus region and development of nanoindentation linescan techniques, Polym. Test. 29 (2010) 494–502, https://doi.org/10.1016/j.polymertesting.2010.02.010.
[4] N. Zinkovska, J. Smilek, M. Pekar, Gradient hydrogels — the state of the art in preparation methods, Polymers 12 (2020) 966–979.
[5] C. Li, L. Ouyang, I.J. Pence, A.C. Moore, Y. Lin, C.W. Winter, J.P.K. Armstrong, M.M. Stevens, Buoyancy-driven gradients for biomaterial fabrication and tissue engineering, Adv Mater 31 (2019), e1900291, https://doi.org/10.1002/adma.201900291.
[6] S.J. Banik, N.J. Fernandes, P.C. Thomas, S.R. Raghavan, A new approach for creating polymer hydrogels with regions of distinct chemical, mechanical, and optical properties, Macromolecules 45 (2012) 5712–5717, https://doi.org/10.1021/ma300859b.
[7] J.Y. Wong, A. Velasco, P. Rajagopalan, Q. Pham, Directed movement of vascular smooth muscle cells on gradient-compliant hydrogels, Langmuir 19 (2003) 1908–1913.
[8] S. Gharazi, B.C. Zarket, K.C. DeMella, S.R. Raghavan, Nature-inspired hydrogels with soft and stiff zones that exhibit a 100-fold difference in elastic modulus, ACS Appl. Mater. Interfaces 10 (2018) 34664–34673, https://doi.org/10.1021/acsami.8b14126.
[9] A.A. Mohammed, J. Aviles Milan, S. Li, J.J. Chung, M.M. Stevens, T.K. Georgiou, J.R. Jones, Open vessel free radical photopolymerization of double network gels for biomaterial applications using glucose oxidase, J. Mater. Chem. B. 7 (2019) 4030–4039, https://doi.org/10.1039/c9tb00658c.
[10] A.A. Mohammed, A. Pinna, S. Li, T. Sang, J.R. Jones, Auto-catalytic redox polymerisation using nanoceria and glucose oxidase for double network hydrogels, J. Mater. Chem. B. 8 (2020) 2834–2844, https://doi.org/10.1039/c9tb02729g.
[11] J.P. Gong, Y. Katsuyama, T. Kurokawa, Y. Osada, Double-network hydrogels with extremely high mechanical strength, Adv. Mater. 15 (2003) 1155–1158, https://doi.org/10.1002/adma.200304907.
[12] A. Haque, T. Kurokawa, J. Ping, Super tough double network hydrogels and their application as biomaterials, Polymer (Guildf) 53 (2012) 1805–1822, https://doi.org/10.1016/j.polymer.2012.03.013.
[13] K. Migacz, J. Chlopek, A. Morawska-Chochol, M. Ambroziak, Gradient composite materials for artificial intervertebral discs, Acta Bioeng. Biomech. 16 (2014) 3–12, https://doi.org/10.5277/abb140301.
[14] A. Spinnrock, M. Martens, F. Enders, K. Boldt, H. Cölfen, Controlled preparation of nanoparticle gradient materials by diffusion, Nanomaterials 9 (2019), https://doi.org/10.3390/nano9070988.
[15] B.M. Novak, Hybrid nanocomposite materials - between inorganic glasses and organic polymers, Adv. Mater. 5 (1993), https://doi.org/10.1002/adma.19930050603.
[16] C. Sanchez, P. Belleville, M. Popall, L. Nicole, Applications of advanced hybrid organic-inorganic nanomaterials: from laboratory to market, Chem. Soc. Rev. 40 (2011) 696–753.
[17] O. Mahony, O. Tsigkou, C. Ionescu, C. Minelli, L. Ling, R. Hanly, M.E. Smith, M.M. Stevens, J.R. Jones, Silica-gelatin hybrids with tailorable degradation and mechanical properties for tissue regeneration, Adv. Funct. Mater. 20 (2010) 3835–3845.
[18] K. Tsuru, S. Hayakawa, A. Osaka, Synthesis of bioactive and porous organic-inorganic hybrids for biomedical applications, J. Sol. Gel Sci. Technol. 32 (2004) 201–205, https://doi.org/10.1007/s10971-004-5789-1.
[19] L.S. Connell, F. Romer, M. Suárez, E.M. Valliant, Z. Zhang, P.D. Lee, M.E. Smith, J. V Hanna, J.R. Jones, Chemical characterisation and fabrication of chitosan–silica hybrid scaffolds with 3-glycidoxypropyl trimethoxysilane, J. Mater. Chem. B. 2 (2014) 668–680, https://doi.org/10.1039/c3tb21507e.
[20] Y. Shirosaki, T. Okayama, K. Tsuru, S. Hayakawa, A. Osaka, Synthesis and cytocompatibility of porous chitosan-silicate hybrids for tissue engineering

scaffold application, Chem. Eng. J. 137 (2008) 122–128, https://doi.org/10.1016/j.cej.2007.10.012.
[21] G. Poologasundarampillai, C. Ionescu, O. Tsigkou, M. Murugesan, R.G. Hill, M.M. Stevens, J. V Hanna, M.E. Smith, J.R. Jones, Synthesis of bioactive class II poly(γ-glutamic acid)/silica hybrids for bone regeneration, J. Mater. Chem. 20 (2010) 8952, https://doi.org/10.1039/c0jm00930j.
[22] J.R. Jones, Review of bioactive glass: from Hench to hybrids, Acta Biomater. 9 (2013) 4457–4486, https://doi.org/10.1016/j.actbio.2012.08.023.
[23] F. Tallia, L. Russo, S. Li, A.L.H. Orrin, X. Shi, S. Chen, J.A.M. Steele, S. Meille, J. Chevalier, P.D. Lee, M.M. Stevens, L. Cipolla, J.R. Jones, Bouncing and 3D printable hybrids with self-healing properties, Mater, Horizons 5 (2018) 849–860, https://doi.org/10.1039/c8mh00027a.
[24] J. Deng, Y. Wu, Green synthesis and biomedical properties of novel hydroxypropyl cellulose-g-polytetrahydrofuran graft copolymers with silver nanoparticles, Ind. Eng. Chem. Res. 59 (2020) 732–742, https://doi.org/10.1021/acs.iecr.9b04799.
[25] H.Y. Mi, X. Jing, B.N. Napiwocki, B.S. Hagerty, G. Chen, L.S. Turng, Biocompatible, degradable thermoplastic polyurethane based on polycaprolactone-block -polytetrahydrofuran- block -polycaprolactone copolymers for soft tissue engineering, J. Mater. Chem. B. 5 (2017) 4137–4151, https://doi.org/10.1039/c7tb00419b.
[26] M. Kamitakahara, M. Kawashita, N. Miyata, T. Kokubo, T. Nakamura, Preparation of bioactive flexible poly(tetramethylene oxide) (PTMO)-CaO-Ta2O5 hybrids, J. Mater. Sci. Mater. Med. 18 (2007) 1117–1124, https://doi.org/10.1007/s10856-007-0147-9.
[27] W. Fan, T. Du, A. Droce, L.R. Jensen, R.E. Youngman, X. Ren, L. Gurevich, M. Bauchy, P. Kristensen, B. Xing, D. Yu, M.M. Smedskjaer, Resolving the conflict between strength and toughness in bioactive silica–polymer hybrid materials, ACS Nano (2022), https://doi.org/10.1021/acsnano.2c03440.
[28] M. Aghayan, P. Alizadeh, M. Keshavarz, Multifunctional polyethylene imine hybrids decorated by silica bioactive glass with enhanced mechanical properties, antibacterial, and osteogenesis for bone repair, Mater. Sci. Eng. C. 131 (2021), 112534, https://doi.org/10.1016/j.msec.2021.112534.
[29] W. Fan, R.E. Youngman, X. Ren, D. Yu, M.M. Smedskjaer, Structural control of self-healing silica–poly(tetrahydropyran)–poly(ε-caprolactone) hybrids, J. Mater. Chem. B. 9 (2021) 4400–4410, https://doi.org/10.1039/d1tb00555c.
[30] J.J. Chung, S. Li, M.M. Stevens, T.K. Georgiou, J.R. Jones, Tailoring mechanical properties of sol–gel hybrids for bone regeneration through polymer structure, Chem. Mater. 28 (2016) 6127–6135, https://doi.org/10.1021/acs.chemmater.6b01941.
[31] N. Miyata, K. Fuke, Q. Chen, M. Kawashita, T. Kokubo, T. Nakamura, Apatite-forming ability and mechanical properties of PTMO-modified CaO–SiO2 hybrids prepared by sol–gel processing: effect of CaO and PTMO contents, Biomaterials 23 (2002).
[32] T. Sang, S. Li, H.-K. Ting, M.M. Stevens, C.R. Becer, J.R. Jones, Hybrids of Silica/Poly(caprolactone coglycidoxypropyl trimethoxysilane) as Biomaterials, Chem. Mater. 30 (2018) 3743–3751, https://doi.org/10.1021/acs.chemmater.8b00751.
[33] F. Tallia, J.R. Jones, L. Cipolla, L. Russo, G.R. Young, Hybrid Materials and Process for Production Thereof - Invention Specifications GB 1605446, vol. 2, 2019.
[34] S.A. Ferreira, M.S. Motwani, P.A. Faull, A.J. Seymour, T.T.L. Yu, M. Enayati, D.K. Taheem, C. Salzlechner, T. Haghighi, E.M. Kania, O.P. Oommen, T. Ahmed, S. Loaiza, K. Parzych, F. Dazzi, O.P. Varghese, F. Festy, A.E. Grigoriadis, H.W. Auner, A.P. Snijders, L. Bozec, E. Gentleman, Bi-directional cell-pericellular matrix interactions direct stem cell fate, Nat. Commun. 9 (2018) 4049, https://doi.org/10.1038/s41467-018-06183-4.
[35] S.A. Ferreira, P.A. Faull, A.J. Seymour, T.T.L. Yu, S. Loaiza, H.W. Auner, A.P. Snijders, E. Gentleman, Neighboring cells override 3D hydrogel matrix cues to drive human MSC quiescence, Biomaterials 176 (2018) 13–23, https://doi.org/10.1016/j.biomaterials.2018.05.032.
[36] D. Tian, P. Dubois, R. Jérôme, Biodegradable and biocompatible inorganic-organic hybrid materials. I. Synthesis and characterization, J. Polym. Sci. Part A Polym. Chem. 35 (1997) 2295–2309, https://doi.org/10.1002/(SICI)1099-0518(199708)35:11<2295::AID-POLA21>3.0.CO;2-8.
[37] D. Tian, S. Blacher, P. Dubois, R. Jérôme, Biodegradable and biocompatible inorganic-organic hybrid materials 2. Dynamic mechanical properties, structure and morphology, Polymer (Guildf) 39 (1998) 855–864, https://doi.org/10.1016/S0032-3861(97)00343-1.
[38] G.R. Fulmer, A.J.M. Miller, N.H. Sherden, H.E. Gottlieb, A. Nudelman, B.M. Stoltz, J.E. Bercaw, K.I. Goldberg, NMR chemical shifts of trace impurities: common laboratory solvents, organics, and gases in deuterated solvents relevant to the organometallic chemist, Organometallics 29 (2010) 2176–2179, https://doi.org/10.1021/om100106e.
[39] A.L. Macon, S.J. Page, J.J. Chung, N. Amdursky, M.M. Stevens, J. V Weaver, J. V Hanna, J.R. Jones, A structural and physical study of sol-gel methacrylate-silica hybrids: intermolecular spacing dictates the mechanical properties, Phys. Chem. Chem. Phys. 17 (2015) 29124–29133, https://doi.org/10.1039/c5cp04656d.
[40] G. Poologasundarampillai, B. Yu, O. Tsigkou, D. Wang, F. Romer, V. Bhakhri, F. Giuliani, M.M. Stevens, D.S. McPhail, M.E. Smith, J. V Hanna, J.R. Jones, Poly(gamma-glutamic acid)/silica hybrids with calcium incorporated in the silica network by use of a calcium alkoxide precursor, Chem. Eur J. 20 (2014) 8149–8160, https://doi.org/10.1002/chem.201304013.
[41] H.J. Lee, K.S. Oh, C.K. Choi, The mechanical properties of the SiOC(-H) composite thin films with a low dielectric constant, Surf. Coating. Technol. 171 (2003) 296–301, https://doi.org/10.1016/s0257-8972(03)00289-5.
[42] X. Zhang, Y. Wu, S. He, D. Yang, Structural characterization of sol–gel composites using TEOS/MEMO as precursors, Surf. Coating. Technol. 201 (2007) 6051–6058, https://doi.org/10.1016/j.surfcoat.2006.11.012.
[43] T.G. Tienen, R.G. Heijkants, J.H. de Groot, A.J. Pennings, A.J. Schouten, R.P. Veth, P. Buma, Replacement of the knee meniscus by a porous polymer implant: a study in dogs, Am. J. Sports Med. 34 (2006) 64–71, https://doi.org/10.1177/0363546505280905.
[44] B.J.M. Pol, P.B. Van Wachem, M.J.A. Van Luyn, L. Van der Does, A. Bantjes, In vivo testing of crosslinked polyethers. I. Tissue reactions and biodegradation, J. Biomed. Mater. Res. 32 (1996) 307–320.
[45] B.J.M. Pol, P.B. van Wachem, L. van der Does, A. Bantjes, In vivo testing of crosslinked polyethers. II. Weight loss, IR analysis, and swelling behavior after implantation, J. Biomed. Mater. Res. 32 (1996) 321–331.
[46] H.-J. Wilke, P. Neef, M. Caimi, T. Hoogland, L.E. Claes, New in vivo measurements of pressures in the intervertebral disc in daily life, Spine (Phila. Pa. 24 (1999) (1976) 755–762.